RADIAL GAS FRACTION PROFILES IN VERTICAL PIPE FLOW

Eckhard Krepper, Dirk Lucas and Horst-Michael Prasser

1. Introduction

One-dimensional codes are frequently used for the simulation of two phase flow in the field of design, optimization and safety analysis of nuclear and chemical plants. Most of the correlations used by these codes e.g. for pressure drop or heat and mass transfer are valid only for a given flow regime. The definition of these flow regimes is based on steady state flow regime maps. Steady state flow maps, however are not able to predict the flow pattern in case of transient flows. Recently attempts were made to solve this problem by the introduction of additional equations for the bubble density or corresponding parameters like bubble diameter, bubble volume or interfacial area. Bubble coalescence and break-up rates, which form the source terms in these equations, are determined by local events. That means, they depend on local parameters of turbulence as well as on the local bubble size distribution.

Forces acting on bubbles in a gas-liquid flow strongly depend on the bubble diameter. This is well known for the drag force, which was investigated by many authors. In the field of the so-called non-drag forces, which act perpendicular to the flow direction, there are still open questions. Recently, it was found, that the lift force changes its sign at some critical bubble diameter [1], e.g. in a vertical upwards pipe flow, small bubbles are moved towards the wall, while bubbles with a diameter greater than the critical migrate towards the centre of the tube. Concerning the other non-drag forces, i.e. the lubrication force and the turbulent dispersion force, there are also still needs to complete the models.

The experimental input for the study of these forces comes mainly from the observation of single bubbles. In this paper a method is introduced, that allows to effectively analyse the motion of bubbles depending on their size in a multi-disperse flow. For this purpose, measurements applying a wire-mesh sensor developed in Forschungszentrum Rossendorf [2], [3] in a vertical upwards flow were carried out. A method to measure bubble size distributions by evaluating wire-mesh sensor data was presented [4]. The bubble identification algorithm can be used to decompose radial gas fraction profiles according to bubble size classes. Measurements taken at different distances from a gas injection show the evolution of the gas fraction profiles for different bubble size classes separately. This makes it possible to study the net motion of the bubbles in the direction perpendicular to the flow, and to check theoretical models of the non-drag forces in a realistic multi-disperse flow [5].

A one-dimensional model is presented, which predicts the radial volume fraction profiles from a given bubble size distribution [6]. It bases on the assumption of equilibrium of the non drag forces acting on a bubble perpendicularly to the flow path. This model together together with appropriate models for local bubble coalescence and break-up could be used for the prediction of the flow pattern.

2. The experiments

2.1. Processing of the wire-mesh sensor data

The tests were performed to study the evolution of the bubble size distribution in a vertical tube of 51.2 mm diameter. Air-water flow at a temperature of 30 °C was investigated. The superficial velocities were varied in the range of $0 < J_{gas} < 4$ m/s and $0 < J_{liquid} < 12$ m/s. The distance between sensor and air injection was varied from 0.03 m to 3.5 m. This corresponds to related inlet lengths of 0.6 = L/D = 70.

The wire-mesh sensor delivers a sequence of two-dimensional distributions of the local instantaneous conductivity, measured in each mesh formed by two crossing wires (see [3], [4]). Local instantaneous gas fractions are calculated assuming a linear dependence between gas fraction and conductivity. The result is a three-dimensional data array (i,j,k where k is the number of the instantaneous gas fraction distribution in the time sequence. The indices correspond to co-ordinates x,y of the local measurement in the cross section and the time t. $t = k \cdot \Delta t$. Averaging the local gas fractions over the time, radial gas fraction profiles, i.e. average gas fractions in dependence on the distance from the tube centre may be determined. In the case of steady flow conditions, the time axis can be transformed into a virtual z*-axis by scaling it with the average phase velocity of the gaseous phase: $z^x = \overline{w_{gas}} t \cong t \cdot J_{gas} / \bar{\varepsilon}$.

At moderate flow velocities, the high time resolution allows to perform a bubble size measurement, because individual bubbles are mapped in several successive frames. Furthermore, gas fraction portions belonging to bubbles the dimensions of which exceed the electrode pitch are found in more than one mesh of the sensor. A detailed description of the method can be found in [4] or [5].

2.2. Decomposition of radial gas fraction profiles

The bubble identification algorithm allows to identify the elements [i,j,k] of the gas fraction distribution $\varepsilon_{i,j,k}$ that belong to a given bubble. Since the bubble diameter is known after the summation of all elements, it is possible to decompose the gas fraction distribution according to the belonging bubble diameter. Partial radial gas fraction profiles are obtained, which consider only bubbles from a given range of diameters [5].

The left column of Fig. 1 represents a virtual sectional side view of the sequence of gas fraction distributions measured by the sensor. The upper

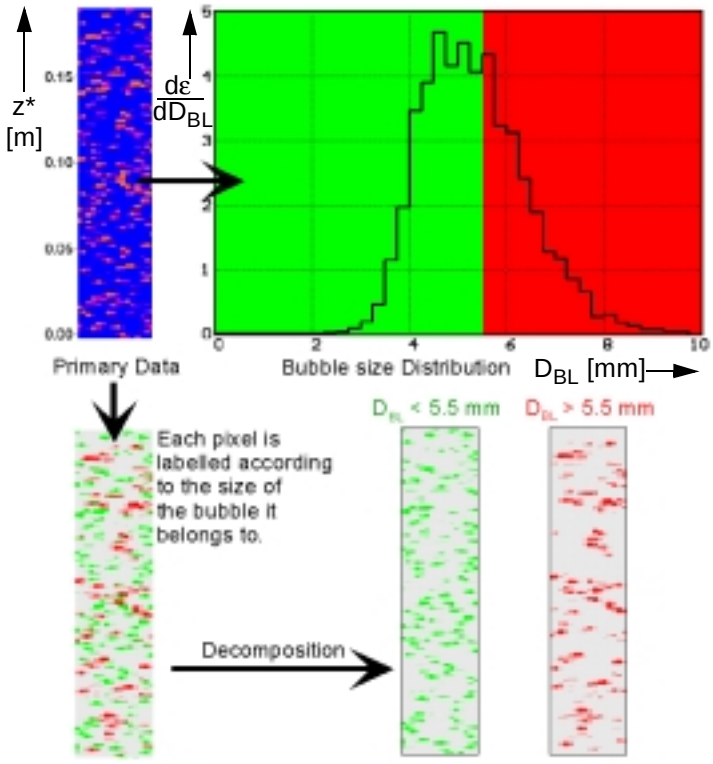

Fig. 1: Decomposition of radial gas fraction profiles according to the bubble size

right plot shows the bubble size distribution. In the lower left column the bubbles are labelled according to their diameter: If the diameter is less than 5.5 mm, they are painted green, in the opposite case red. Now, the initial sequence can be divided in sequences of gas fraction distributions considering only bubbles with $D_{bub} < 5.5$ mm (column with only green bubbles) and $D_{bub} > 5.5$ mm (column with only red bubbles). These decomposed data sets are taken to calculate time averaged gas fraction distributions.

2.3. Influence of primary gas fraction profile and primary bubble size distribution on the evolution of the two-phase flow

Three different types of air injecting devices were used (see Fig. 2): A - an array of 19 capillaries of 0.8 mm inner diameter, the ends of which were bent into the flow direction and equally distributed over the cross section, B - 36 orifices in the tube side wall with 1 mm inner diameter and C - 8 orifices in the side wall of 4 mm diameter.

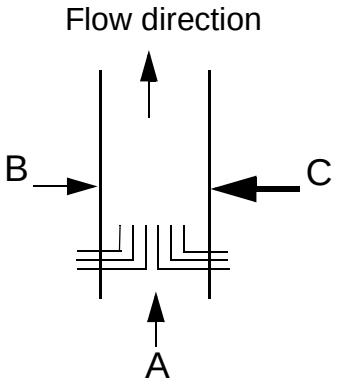

Fig. 2: Investigated injection devices

The described decomposition of radial gas fraction profiles was applied to data obtained in experiments at superficial velocities of J_{liquid} = 0.4 m/s and J_{gas} = 0.06 m/s, which were carried out with all three air injection devices (see Fig. 3). The inlet length was varied from L/D = 0.6 (H = 30 mm) to L/D = 60 (H = 3133 mm).

The measured bubble size distribution at L/D = 0.6 indicates, that in case of injection A all primary bubbles have an equivalent diameter smaller than 5.5 mm. The gas injection through the 1 mm orifices in the wall also produces small bubbles with a diameter mainly below 5.5 mm, while the 4 mm orifices generate larger primary bubbles of about 8 mm. Along the flow path, the bubble size distributions remain almost constant in case of injection A and B, while the larger bubbles produced by the 4 mm orifices (C) start to coalesce. The bubble size distribution is changed from the initial mono-modal one to a bimodal. Both large bubbles of about 30 mm diameter as well as small bubbles with a diameter significantly less than the initial bubble diameter are found at the end of the test section (L/D=60).

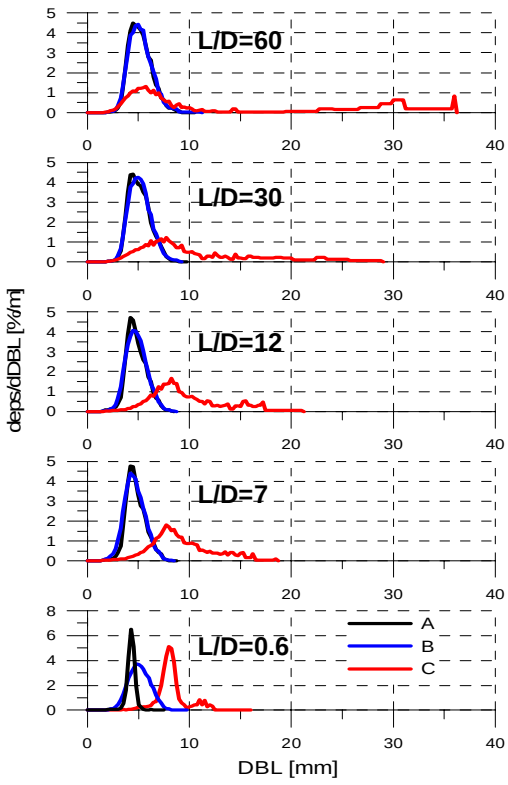

Fig. 3: Bubble size distribution (J_{liquid}=0.4m/s; J_{gas}=0.06m/s)

In case of the capillary injection (A), bubbles larger than the critical diameter of 5.5 mm are not present in the initial distribution. The decomposed radial gas fraction profiles in Fig. 4 clearly show the tendency of the small bubble fraction to move towards the wall. At H = 30 mm, the profile is still

strongly determined by the gas fraction maxima found at the places where capillaries are located. With growing distance, the gas fraction represented by the small bubble fraction shifts towards the wall. The increase of gas fraction near the wall leads to an intensification of coalescence, which leads to a generation of bubbles with D_{bub} > 5.5 mm in this region. These bubbles experience an inverse lift force, pushing them towards the centre of the pipe. A pronounced wall peaking of the total gas fraction profile is observed, caused by the peak of the partial gas fraction of the small bubble class. The large bubbles (D_{bub} > 5.5 mm) tend to form a central maximum. Despite of the completely different initial gas fraction profile produced by the equally distributed capillaries (A) and the wall orifices of 1 mm diameter (B), the decomposed radial profiles converge with growing distance (Fig. 4). At a relative length of L/D 60, the profiles become identical.

The gas fraction profiles obtained for the injection device C (4 mm orifices) behave completely different. Here, the primary bubbles are larger than 5.5 mm. Closely above the injection they are still found at the periphery, since they have been generated at the wall. With growing height, a generation of bubbles smaller than 5.5 mm and larger that 12.5 mm is observed. Since bubbles with a diameter less than 5.5 mm are not generated at the gas injection orifices, they must be the result of fragmentation events. Bubbles larger than 12.5 mm are the result of coalescence. The bubbles of both classes of large bubbles (5.5 mm < D_{bub} < 12.5 mm and

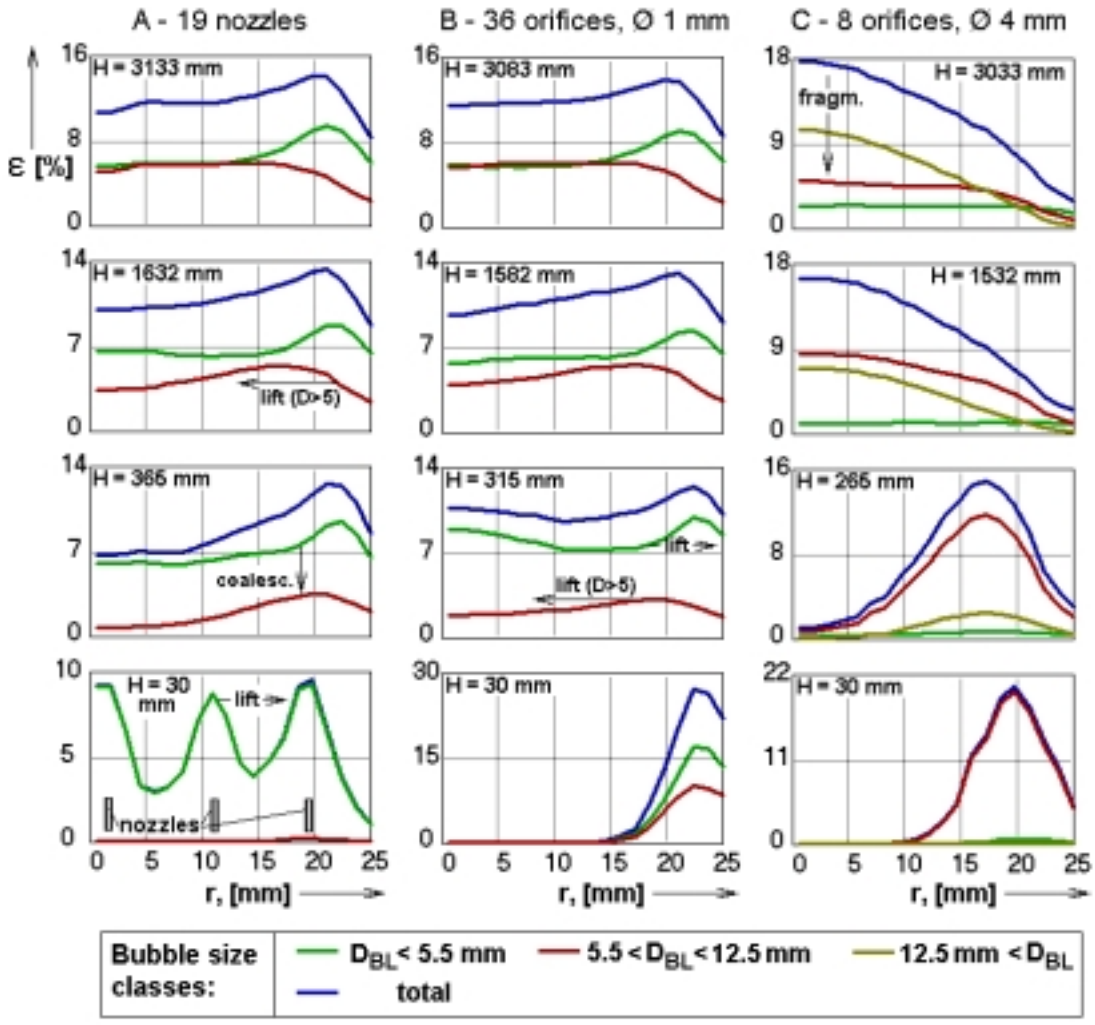

Fig. 4: Measured bubble radial gas fraction distribution

12.5 mm < D_{bub}) are quickly shifted to the centre of the pipe. Although the small bubbles are transported towards the wall, they are almost uniformly distributed at the end of the test section. This can be explained by a source of small bubbles due to fragmentation in the central region.

During the test presented in Fig. 4, injection device B and C represent the same primary gas fraction profile and device A and B the same primary bubble size distribution. In Fig. 4 the gas fraction profile at the end of the tube is almost the same for injection devices A and B. That means, that the primary bubble size distribution has a larger influence on the evolution of the two phase flow than the primary gas fraction profile.

3. The model

Forces acting perpendicular to the flow direction determine the formation of radial distributions of the bubbles. The classical lift force is shear-induced and acts toward the wall. Related on the unit volume it can be calculated as

$$\overrightarrow{F_L} = -C_L \rho_L (\overrightarrow{w_g} - \overrightarrow{w_l}) \times rot(\overrightarrow{w_l}) \tag{1}$$

with a positive lift force coefficient C_L. ρ_L is the liquid density, w_g and w_l the gas respective the liquid velocity. Tomiyama et al. [1] proposed another kind of transverse lift force, which is caused by the interaction between the wake and the shear field. It acts to the opposite direction, that means it is also calculated by equation (1), but has a negative coefficient C_L. Tomiyama expresses both forces summarized as a net transverse lift force with the experimentally determined coefficient C_T, which depends on the bubble Eötvös number. For the water-air system at normal conditions C_T changes its sign at the bubble diameter D_{bub}=5.8 mm, i.e. the net transverse lift force acts towards the wall for bubbles with a diameter less than 5.8 mm and it acts towards the pipe centre for larger bubbles.

The lubrication force, introduced by Antal et al. [7], drives bubbles away from the wall. Tomiyama [1] developed an modified equation for this force per unit volume:

$$\overrightarrow{F_W} = -C_W \frac{D_{bub}}{2} \left(\frac{1}{(R-r)^2} - \frac{1}{(R+r)^2} \right) \rho_l w_{rel}^2 \overrightarrow{n_r} \tag{2}$$

with w_{rel} as the velocity difference between liquid and gas, R the tube radius and r the distance of the bubble from the tube centre. $\overrightarrow{n_r}$ is the normal vector to the wall. The coefficient C_W also depends on the Eötvös number.

The model does not consider single bubbles, but the radial distributions of volume fractions for single bubble classes. The turbulent dispersion force considers the smoothing of these radial gas profiles caused by turbulence. Lahey et al. [8] derived an equation for the force per unit volume as

$$\overrightarrow{F_D} = -0.1 \rho_l k_l \nabla \alpha \tag{3}$$

with k_l as the turbulent kinetic energy of the liquid and $\nabla\alpha$ the gradient of the gas volume fraction. Following [1] there is a fluctuating motion of single bubbles, which increases with the

Eötvös number. It is caused by the deformation of the bubbles. These fluctuations cause an additional smoothing of the profiles, which is not taken into account by the dispersion force according to equation (3). For this reason a second dispersion force is introduced, which depends on the Eötvös number. As reported in [1] the fluctuations were observed at bubbles with Eötvös numbers larger than about 1. For this reason we stated

$$\overrightarrow{F_{D,\,Eo}} = -C_{D,\,Eo}\rho_l(Eo-1)\nabla\alpha \qquad (4)$$

for the new Eötvös number dependent dispersion force.

The parameter $C_{D,Eo}$ is the only new model parameter. According to integral experimental data (see below) $C_{D,Eo} = 0.0015\ m^2/s^2$ is assumed for Eo>1. For Eo<1 $C_{D,Eo}$ is set to zero.

The radial balance of forces applying equations (1)-(4) results in

$$(0.1k_l + C_{D,\,Eo}(Eo-1))\frac{d\alpha_i}{dr} + \left(C_T w_{rel}\frac{dw_l}{dr} + C_W\frac{D_{bub}}{2}\left(\frac{1}{(R-r)^2} - \frac{1}{(R+r)^2}\right)w_{rel}^2\right)\alpha_i = 0 \qquad (5)$$

This equation is a first order differential equation with respect to the volume fraction of a bubble size class $\alpha_i(r)$. It is solved separately for each bubble class. The sum of these profiles is the radial gas fraction profile. The radial profiles of the turbulent kinetic energy of the liquid k_l and of the gradient of the liquid velocity dw_l/dr are still needed to solve the equation.

The radial profile of the liquid velocity is calculated for a given radial gas distribution using the model of Sato et al. [9]. They subdivided the eddy diffusivity into a component, which considers the inherent wall turbulence and a component, which considers the turbulence caused by the bubbles. This causes a feedback between the radial gas profile and the radial profile of liquid velocity. The complete model equations as well as a scheme for a numerical solution procedure can be found in [9].

For the calculation of the turbulent kinetic energy the equations of the k-ε model are used. A common non-linear differential equation of second order for the steady state turbulent kinetic energy k of the liquid can be derived using the following assumptions:

- The time averaged liquid velocity has only a component in axial direction.
- The time averaged liquid velocity is only a function of the radius and does not depend on the azimuthal position and the height.

There is a very sensitive feedback between the velocity profile and the gas fraction profile. For this reason they are calculated within an iteration procedure. An underrelaxation is necessary to guarantee the stability of the iteration. Calculations with an assumed velocity profile according to a 1/m-law typical for turbulent flow through a tube have shown, that this feedback is not negligible. In case of a flow with bubble sizes below 5.8 mm the feedback smoothe the radial gas profiles. The bubbles are located preferably at the wall. For this reason the liquid velocity near to the wall is increased. This smoothe the velocity profile apart from the wall and reduces the lift force in the core region of the flow, which acts towards the wall. Otherwise, if a considerable fraction of bubbles with a diameter larger than 5.8 mm occurs, there is a positive feedback between the gas and velocity profiles. The bubbles in the centre accelerate the liquid. For this reason the velocity gradient in the central region increases. This again causes an

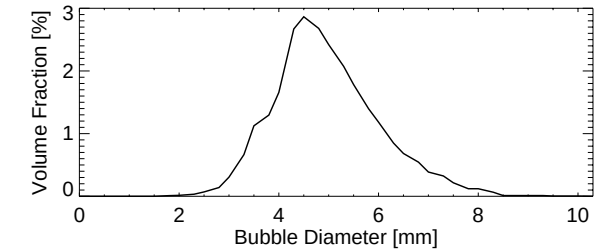

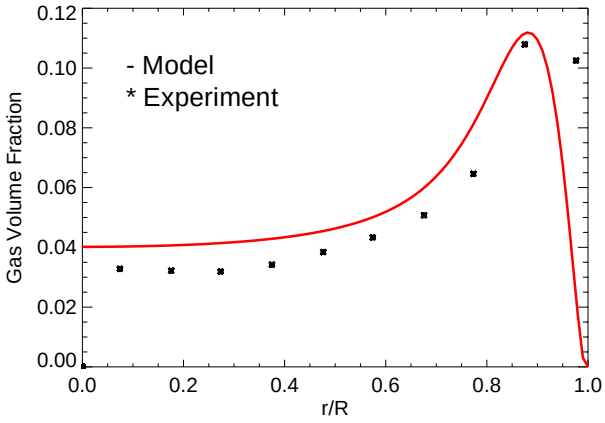

Fig. 5: Measured bubble size distribution and radial gas profiles J_{liquid} = 1.0167 m/s, J_{gas} = 0.0574 m/s

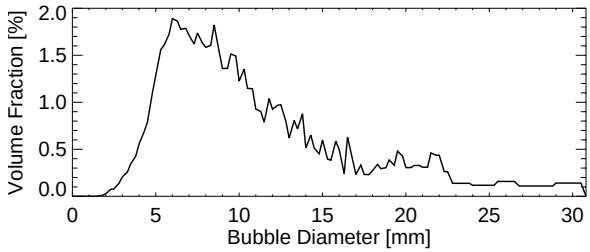

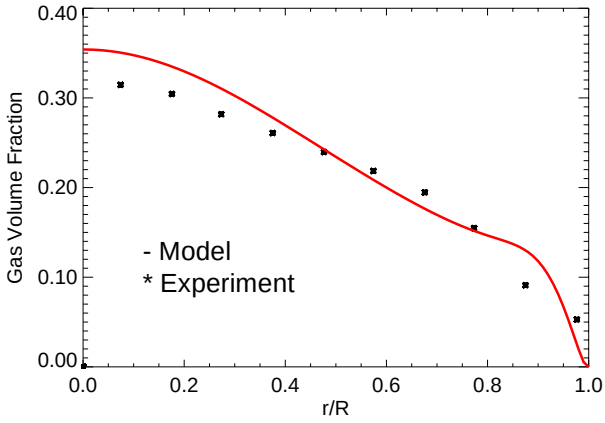

Fig. 6: Measured bubble size distribution and radial gas profiles J_{liquid} = 1.0167 m/s, J_{gas} = 0.219 m/s

increase of the lift force, which acts bubbles with a diameter larger than 5.8 mm towards the pipe centre in the calculation. The turbulent component of the dispersion force is not strong enough to distribute the large bubbles over the cross section of the pipe. Obviously, another mechanism is dispersing the bubbles. The fluctuating motion of the large bubbles, as observed by Tomiyama [1], may be such a mechanism. Therefore the additional dispersion force according to equation (4) was introduced. The parameter $C_{D,Eo}$ was tuned to achieve a good agreement between calculated and measured radial profiles for large bubbles.

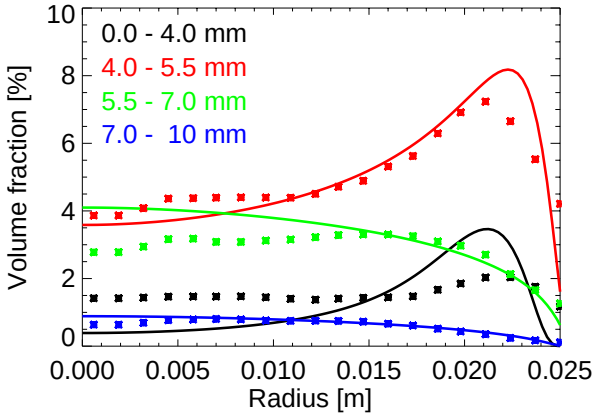

Fig. 7: Comparison of radial volume fraction profiles for bubbles of different size. stars: experiment, solid line: model, J_{liquid} = 0.4 m/s, J_{gas} =0.057 m/s

The results of the model were compared with experimental data for a number of gas and liquid superficial velocities. Measured bubble size distributions were taken as an input for the model. There is a good agreement between experimental and calculated radial profiles. In particular the change from wall peaking to central peaking is well predicted. As an example Fig. 5 and Fig. 6 show a comparison of experimental and calculated data. Fig. 7 shows a comparison of radial volume fraction profiles for bubbles of different size. The good agreement confirms the

results from [1] concerning the bubble size dependency of the lift force and following the radial profiles.

4. Conclusions

The presented model allows the prediction of radial gas profiles in vertical pipe flows. In particular the model allows a prediction whether wall peaking or core peaking occurs in dependence of the gas and liquid superficial velocities and the bubble size distribution. The good agreement between experimental and calculated data confirms the dependency of the radial forces acting on a bubble on the bubble size as reported by Tomiyama [1]. The correlations for these forces as well as the model for the radial velocity profile were taken from literature without any change of the empirical parameters. The only extension was the introduction of a Eötvös number dependent dispersion force. The dependency of radial forces on bubble size is very important for the modelling of the transition between bubble flow and slug flow. It is supposed, that the attempts for a one-dimensional modelling of bubble coalescence and bubble break-up suffer from neglecting the radial profiles of the particle densities for the single bubble classes. This assumption will be proofed in a next step by including correlations for bubble coalescence and break-up into the presented model. Further it will be proofed, whether a few-zone model (e.g. core region - wall region) is sufficient to reflect the radial profiles. Such a model could be used in one-dimensional transport codes.

References

[1] A. Tomiyama (1998), Struggle with computational bubble dynamics, Third International Conference on Multiphase Flow, ICMF'98, Lyon, France, June 8-12, 1998

[2] H.-M. Prasser, A. Böttger, J. Zschau (1998), A new electrode-mesh tomograph for gas-liquid flows, Flow Measurement and Instrumentation 9, 111-119

[3] H.-M. Prasser (1999), Wire-Mesh Sensors for Two-Phase Flow Investigations, in F.-P. Weiß, U. Rindelhardt (Ed.) Annual Report 1998 Institute of Safety Research, pp. 23-28

[4] H.-M. Prasser, D. Scholz, C. Zippe (2001), Bubble Size Measurement using Wire-Mesh Sensors, Flow Measurement and Instrumentation (submitted).

[5] H.-M. Prasser, E. Krepper, D. Lucas (2000), Fast wire-mesh sensors for gas-liquid flows and decomposition of gas fraction profiles according to bubble size classes, 2nd Japanese-European Two-Phase Flow Group Meeting Tsukuba, Japan, September 25-29, 2000

[6] Lucas, D.; Krepper, E.; Prasser, H.-M. (2000), Influence of the bubble size distribution on radial gas fraction profiles in vertical pipe flow, 2nd Japanese-European Two-Phase Flow Group Meeting Tsukuba, Japan, September 25-29, 2000

[7] S.P. Antal, R.T. Lahey, J.E. Flaherty (1991), Analysis of phase distribution in fully developed laminar bubbly two-phase flow, International Journal of Multiphase Flow 17, 635-652

[8] R.T. Lahey, M. Lopez de Bertodano, O.C. Jones (1993), Phase distribution in complex geometry conduits, Nuclear Engineering and Design 141, 177-201

[9] Y. Sato, M. Sadatomi, K. Sekoguchi (1981), Momentum and heat transfer in two-phase bubble flow-I, International Journal of Multiphase Flow 7, 167-177